Journal of the Ceramic Society of Japan 118 [2] 147-151 2010 **Paper**

Photo-initiation of ZnO nanorod formation by femtosecond laser irradiation

Nan WU, Yasuhiko SHIMOTSUMA,*,† Masayuki NISHI, Masaaki SAKAKURA,* Kiyotaka MIURA and Kazuyuki HIRAO

Department of Material Chemistry, Kyoto University, Kyotodaigaku-Katsura, Nisikyo-ku, Kyoto 615−8510
***Innovative Collaboration Center, Kyoto University, Kyotodaigaku-Katsura, Nisikyo-ku, Kyoto 615−8510**

A photo-initiated process via femtosecond pulse induced heterogeneous nucleation in zinc ammine complex ($Zn(NH_3)_4^{2+}$) based aqueous solution without catalyst and surfactant, followed by thermal treatments for crystal growth into zinc oxide (ZnO) nanorods, was investigated. Hexagonal ZnO nanorods of diameter ≤ 100 nm with smooth planes and length ≤ 1 μm were grown with laser irradiation and successive thermal treatment. The studies show that pH value in the aqueous solutions remarkably effect on morphology of the ZnO nanostructure. Due to the localized high supersaturation of precursor, the hexagonal nucleation was induced by laser irradiation.

Key-words : Zinc oxide, Nanorods, Laser processing, Ultrafast pulse, Growth mechanism

[Received October 21, 2009; Accepted December 17, 2009]

1. Introduction

Zinc oxide (ZnO) nanostructures have attracted immense attention as they offer a wide bandgap and a large exciton binding energy of 3.37 eV and 60 meV, respectively, at room temperature[1] and ultraviolet emission.[2)–4)] In particular, ZnO 1D nanostructure such as nanowires and nanorods have been successfully synthesized for various applications ranging from nanolaser,[4)] gas sensor,[5)] biosensor,[6)] field-effect transistor,[7)] solar cell[8)] to field emission.[9)] A number of physical and chemical synthesis processes have been employed for the growth of ZnO nanostructures. Some of the physical methods include the thermal evaporation and vapor transport approaches,[4),10)] metal organic vapor-phase epitaxial growth (MOVPE),[11)] molecular beam epitaxy (MBE)[12)] and pulsed laser deposition (PLD),[6)] which are generally based on catalyzed vapor-liquid-solid growth mechanism.[13)] In addition, the simple and low-cost chemical aqueous solution methods with thermal treatment have also been thoroughly studied.[14)–19)] However, these processes require one or more of the following rigorous conditions; high temperature, low pressure, complex procedures, long growing durations or the need for catalysts, which inadvertently get embedded on the tips of the nanostructures, introducing undesirable impurity. Although recent techniques for nucleation of organic[20),21)] and inorganic[22)–24)] materials with an intense femtosecond laser pulses were proposed, the mechanism is not fully understood. Here we present heterogeneous nucleation induced by the femtosecond laser irradiation in zinc ammine complex ($Zn(NH_3)_n^{2+}$) based aqueous solutions at room temperature and pressure. Such photo-initiated nucleation sites are evidently generated in response to an increase in laser irradiation time and pH value, and subsequently grow into nanorods during low temperature thermal treatments, without the need for catalysts.

† Corresponding author: Y. Shimotsuma; E-mail: yshimo@collon1.kuic.kyoto-u.ac.jp

2. Experimental

Aqueous mixture solutions of 0.02 M $ZnCl_2$ and 0.032–0.200 M NH_4OH at pH value ranging from 8.5 to 10.5 alkaline environments were initially prepared. We used femtosecond laser pulses to focus in a liquid cell and efficiently transfer energy into the precursor solution. The initial solution exhibits a slightly white turbidity decreasing with a pH increase because the formation of zinc ammonia complex, which was subjected to femtosecond pulse irradiation at room temperature. The laser radiation in Gaussian mode produced by a regenerative amplified mode-locked Er-doped fiber laser (Cyber laser Inc., 230 fs pulse duration, 1 kHz repetition rate, pulse energy 0.5 mJ/pulse) operating at a wavelength of 780 nm was focused via 20 × (numerical aperture = 0.40) objective into a rectangular quartz vessel of 1 × 1 × 3.5 cm^3 filled with the precursor solution, which was placed on a magnetic stirrer and continuously stirred to maintain homogeneity. Irradiation was performed for 60 min and the solution subsequently transferred into furnace for heat treatments at 80°C or 100°C for 120 min before being cooled down to room temperature. Samples were prepared by drop-casting the solutions onto silicon substrates and allowed to evaporate at room temperature. The grown ZnO particles were analyzed by field emission scanning electron microscopy (JEOL Ltd., JSM–6705F) to study their morphologies. X-ray diffraction (XRD) pattern was collected using Rigaku Rint2500HF to study the crystal structure.

3. Results and discussion

The solid phase stability of $Zn(OH)_2$ in the precursor solution has been determined by the pH value and the concentration of Zn(II) soluble species.[25)] **Figure 1** shows the phase stability diagrams for the $Zn(OH)_2$–NH_3 systems at 25°C. The dashed lines indicate the thermodynamic equilibrium between the various Zn(II) soluble species, which are calculated by the following equilibrium Eqs.(1)–(3).

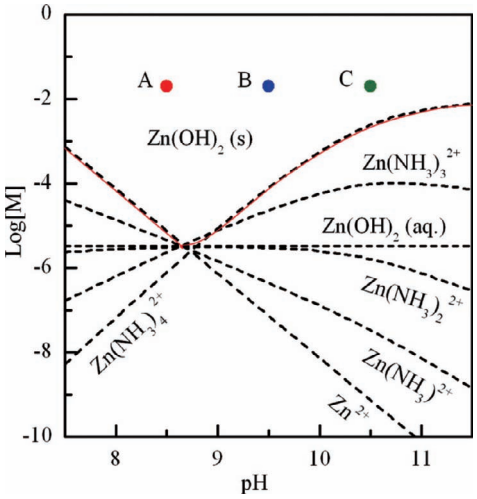

Fig. 1. Phase stability diagram for $Zn(OH)_2$–NH_3 system at 25°C as a function of pH. The points marked by A, B, and C represent the preparation conditions of precursor solution in this study. The dashed lines indicate the thermodynamic equilibrium between the various Zn(II) soluble species and the solid $Zn(OH)_2$. The red solid line represents the boundary of the solubility of the solid $Zn(OH)_2$.

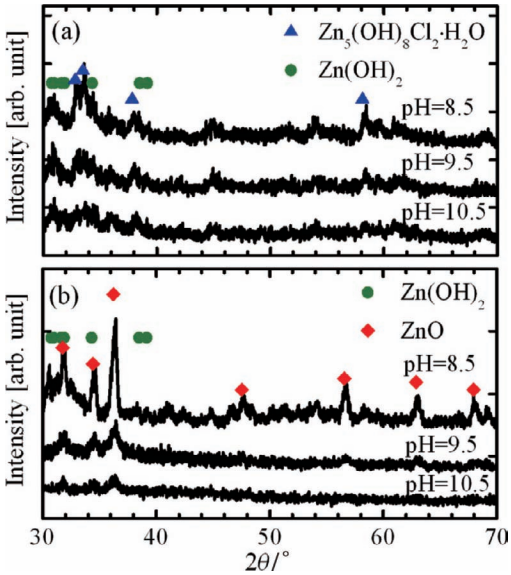

Fig. 2. XRD patterns of precipitates from mixed precursor solutions at pH 8.5, 9.5, and 10.5 without (a) and with (b) the femtosecond laser irradiation for 60 min and the successive thermal treatment at 80°C for 120 min. The JCPDS standards of $Zn_5(OH)_8Cl_2{\cdot}H_2O$ (▲), $Zn(OH)_2$ (●), and ZnO (◆) are also shown.

$$Zn^{2+} + iNH_3 \leftrightarrow Zn(NH_3)_i^{2+} \quad (1)$$

$$Zn(NH_3)_i^{2+} + 2OH^- \leftrightarrow Zn(OH)_2\ (s) + iNH_3 \quad (2)$$

$$Zn(OH)_2\ (s) \leftrightarrow Zn(OH)_2\ (aq.) \quad (3)$$

Values of standard thermodynamic data and stability constant are taken from the literature.[25)–28)] The red solid line represents the boundary of the solubility of the solid $Zn(OH)_2$. This diagram reveals that the solid $Zn(OH)_2$ is thermodynamically stable at a pH value ranging from 7 to 12 in the precursor solutions ($[Zn^{2+}]$ = 0.02 M). Typical three precursor solutions with different pH values of 8.5, 9.5, and 10.5 were prepared in the present study.

Figure 2 XRD patterns of precipitates from mixed precursor solutions of $ZnCl_2$ and NH_4OH at pH 8.5, 9.5, and 10.5 without (a) and with (b) the femtosecond laser irradiation for 60 min and the successive thermal treatment at 80°C for 120 min. The JCPDS standards of $Zn_5(OH)_8Cl_2{\cdot}H_2O$, $Zn(OH)_2$, and ZnO are also shown in Fig. 2. The corresponding SEM micrographs are shown in **Fig. 3**. No apparent diffraction peaks of ZnO were observed in the case of the thermal precipitates from precursor solutions at every pH condition without the laser irradiation (Fig. 2(a)). These patterns were assigned to $Zn(OH)_2$ and $Zn_5(OH)_8Cl_2{\cdot}H_2O$, suggesting that the precursor solutions could not become supersaturated at 80°C with respect to the homogeneous ZnO nucleation. On the other hand, the apparent diffraction peaks attributed to ZnO were observed in the samples which the laser irradiation process was applied before thermal treatment at the same temperature (Fig. 2(b)). This indicates that the photo-initiated heterogeneous nucleation could be induced by the femtosecond laser irradiation in the precursor solutions at room temperature. The SEM images in Fig. 3 evidently indicate that in contrast to the formation of the scale-like or amorphous precipitate after the thermal treatment at 80°C for 120 min, the ZnO hexagonal nanorods with a diameter of 40−80 nm, which slightly decreases with a pH increase, were obtained by applying the laser irradiation (Fig. 3(d)–(f)). Based on these results, we speculated that the nucleations of ZnO nanorods were initiated by the

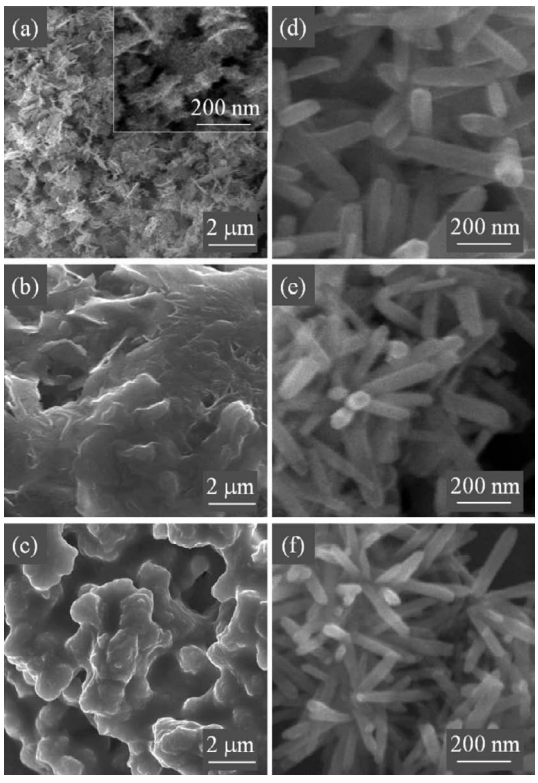

Fig. 3. SEM micrographs of precipitates synthesized from mixed precursor solutions at pH 8.5 (a, d), 9.5 (b, e), and 10.5 (c, f) by the thermal treatment at 80°C for 120 min (left column) and the additional laser irradiation before the thermal treatment (right column). Inset of (a) shows a high magnification image of scale-like particles.

local supersaturation via femtosecond laser pulse irradiation even at the room temperature.

In order to reveal the nucleation and growth mechanisms of

ZnO nanorods with the additional femtosecond laser irradiation process, the heating temperature during the successive thermal treatment was changed to 100°C. ZnO nanoparticles were precipitated with or without laser irradiation (**Fig. 4**). The shape of ZnO nanoparticles was changed from nanorods to flower-like with increasing the pH in the thermal treatment (Figs. 4(a), (c)). In addition, the smaller ZnO nanoparticles resulting from secondary nucleation were observed at the pH of 9.5 (Fig. 4(b)). It is well known that the flower-like ZnO nanostructures are formed via twinned ZnO nuclei along the $(11\bar{2}2)$ planes in the system with higher supersaturation of $Zn(OH)_4^{2-}$.[29] On the other hand, much smaller ZnO nanorods with a diameter of 20–70 nm were formed by the additional laser irradiation compared to that of the thermal process regardless of pH, about 4 times thinner nanorods were especially formed at the pH of 8.5 (Figs. 4(a), (d)). The size of ZnO nanorods obtained by the laser irradiation increased with an increase in pH (Figs. 4(d)–(f)). Comparison of the effect of temperature on the size of ZnO nanorods between 80°C and 100°C with the laser irradiation indicates that the size decreases with increasing temperature at pH of 8.5 and 9.5, although the size increases with increasing temperature at pH of 10.5 (Figs. 3(d)–(f), Figs. 4(d)–(f)).

Based on the difference in the shape and size of ZnO nanostructures with and without the femtosecond laser irradiation before the subsequent thermal treatment, we deduce the formation mechanism of ZnO nanorods below. The possible reactions in our experiments can be summarized in the following Eqs.(4)–(7).

$$Zn^{2+} + 2OH^- \leftrightarrow Zn(OH)_2\ (s) \quad (4)$$

$$Zn(OH)_2\ (s) \rightarrow ZnO + H_2O \quad (5)$$

$$Zn^{2+} + 4NH_3 \leftrightarrow Zn(NH_3)_i^{2+} \quad (6)$$

$$Zn(NH_3)_4^{2+} + 2OH^- \rightarrow ZnO + 4NH_3 + H_2O \quad (7)$$

In the experimental pH region, we could consider the soluble species of the uncomplexed Zn^{2+} ions and the zinc-ammonia complex ions of $Zn(NH_3)_4^{2+}$ at a much higher concentration of NH_3. In addition, the insoluble compounds of $Zn(OH)_2$ can be formed in this system. The calculated concentration of $Zn(NH_3)_4^{2+}$ and solid $Zn(OH)_2$ in mixed precursor solutions are shown in **Table 1**. The size of obtained ZnO nanorods produced by the femtosecond laser irradiation at 0.5 mJ for 60 min and the successive thermal treatment at 100°C for 120 min are also shown. The amount of such precipitation depends on the pH and the concentration of NH_3 in the solution based on the solubility of $Zn(OH)_2$ and the dissociation constants of $Zn(NH_3)_4^{2+}$. At the pH of 8.5 and 9.5, the reaction of Eq.(4) is dominant and the equilibrium moves to right, namely the nuclei of ZnO are predominantly formed from $Zn(OH)_2$ by the laser irradiation. In contrast, a large amount of the soluble complexes ions of $Zn(NH_3)_4^{2+}$ in addition to the precipitation could be consumed by the formation of ZnO nuclei during laser irradiation, because the reaction of Eq.(6) is dominant at the pH of 10.5. Indeed, the energy absorption by the focusing of femtosecond laser pulses was almost same of 66% regardless of the pH, although the scattered light intensities at the pH of 8.5 and 9.5 was about 2.5 times higher than that at the pH of 10.5. During the subsequent thermal treatment after the laser irradiation, ZnO nuclei formed by the different reaction path grow into ZnO nanorods along the *c*-axis direction.[30] In lower pH solution (pH 8.5), the smaller ZnO nanorods are formed by the secondary nucleation and growth during the hydrothermal process (Fig. 4(d)). On the other hand, the larger nanorods could be obtained because ZnO nuclei formed by the laser irradiation grow dominantly during the thermal treatment. It is noted that the standard Gibbs free energy changes of Eq.(5) and (7) are -3.94 and -47.2 kJ/mol, respectively.

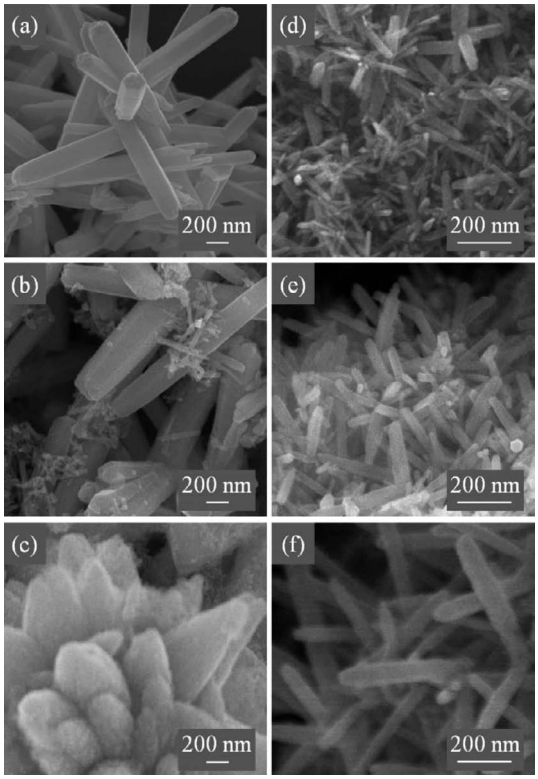

Fig. 4. SEM micrographs of precipitates synthesized from mixed precursor solutions at pH 8.5 (a, d), 9.5 (b, e), and 10.5 (c, f) by the thermal treatment at 100°C for 120 min (left column) and the additional laser irradiation before the thermal treatment (right column).

Table 1. Calculated Concentration of Soluble and Insoluble Zn(II) Species and the Corresponding the Size of Obtained ZnO Nanorods

pH	$Zn(NH_3)_4^{2+}$ [mol/L]	$Zn(OH)_2$ (s) [mol/L]	ZnO nanorods	
			Diameter [nm]	Length [nm]
8.5	8.1×10^{-7}	9.1×10^{-3}	38 (7) [a]	164 (5) [a]
9.5	7.8×10^{-5}	9.1×10^{-3}	44 (5) [a]	233 (3) [a]
10.5	2.4×10^{-3}	6.6×10^{-3}	68 (24) [a]	515 (46) [a]

[a] The numbers in the parenthesis show the standard deviation for 20 samples.

To discuss the dynamics of ZnO nuclei formation during the femtosecond laser irradiation, we measured the evolution of spectral extinction of the precursor solutions during the femtosecond laser irradiation (**Fig. 5**). The transmitted visible light was detected by a photonic multi- channel analyzer (Hamamatsu Photonics, PMA–11). The components of the extinction in Fig. 5 include the sum of light scattering and absorption by ZnO nuclei formed by the laser irradiation. Assuming that the visible absorption of ZnO is negligible, we could estimate the dynamics of the photo-initiated nucleation process based on the Rayleigh scattering theory. In the Rayleigh scattering regime, the scattered light intensity is inversely proportional to the fourth power of wavelength, indicating the shorter wavelength will scatter more

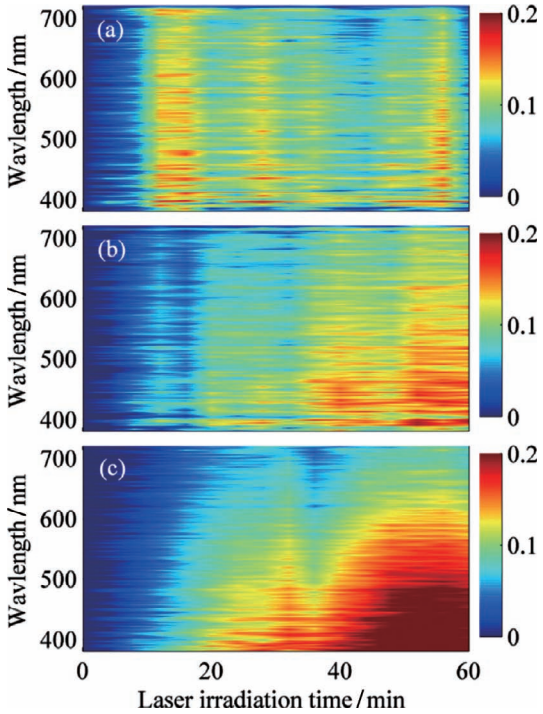

Fig. 5. Evolution of visible extinction spectra of the precursor solution at pH 8.5 (a), 9.5 (b), and 10.5 (c) during femtosecond laser irradiation. The components of the extinction include the sum of light scattering and absorption by ZnO nuclei formed by the laser irradiation.

than the longer wavelength. While the scattered light intensity in the lower pH solution was substantially constant (Fig. 5(a)), in the higher pH solution, the scattered light intensity in the shorter wavelength region increases with an increasing in laser irradiation time (Fig. 5(c)). The results clearly indicate that ZnO nuclei are produced from the liquid phase, i.e. Eq.(6) and (7), in the higher pH solution. On the other hand, the scattering light intensity does not change dramatically because solid $Zn(OH)_2$ already exists in the lower pH solution (Eq.(4) and (5)). Finally, ZnO nuclei produced through different reaction pathways grow into ZnO nanorods during the successive thermal treatment even in the higher pH solution.

In order to understand the origin of the observed phenomenon, the following explanation of the heating mechanism is proposed. Since the light intensity in the focus of the beam is of 10^{16} W/cm^2, the plasma is produced by multiphoton ionization in the focal volume. Once a high free electron density is produced by multiphoton ionization, the material has the properties of plasma and will absorb the laser energy via absorption mechanism of inverse Bremstrahlung heating. Assuming that the electron temperature is proportional to the pulse energy, the electron temperature can be roughly estimated by a simple formula: $Q = C_eVT_e$, where Q ($= \eta E$) is the absorbed energy, η is the absorption coefficient, E is the pulse energy, V is the volume interaction, T_e is the electron temperature, and C_e is the electron heat capacity. Within the free electron gas model, The electron heat capacity can be approximately calculated by $C_e(T_e) = \gamma T_e$, where $\gamma = \pi^2 n_e \kappa_B^2 / 2I_E$,[31] where n_e is the electron number density, κ_B is the Boltzmann constant, I_E is the ionization potential. The electron temperature is estimated to be 1.3 keV (~ 1.5×10^7 K) by using the parameters in **Table 2**, which corresponds to the experimental results.[32] Based on this calculation, not only the optical breakdown, bubble formation, but also the dissociation of the precursor solution could occur within the focal volume during the femtosecond laser irradiation. Such very high electron temperature decreases with an increase of the lattice temperature, then it reaches to the same temperature as lattice temperature with a time scale of several picoseconds. Assuming that the initial temperature of focal volume reaches $\Delta T_0 = 3000$ K after the electron-phonon coupling, the thermal diffusivity can be calculated by the following equation. For simplicity, we used the thermal diffusivity coefficient of distill water ($D_{th} = 1.43 \times 10^{-7}$ m^2/s).

Table 2. Parameter for the Calculation of the Electron Temperature

Material	Water	–
Density, ρ	1.0×10^3	[kg/m^3]
Molar weight, M	1.8×10^{-2}	[kg/mol]
Ionization potential, I_E	6.5	[eV]
Laser wavelength, λ	7.8×10^{-7}	[m]
Pulse width, τ_p	2.3×10^{-13}	[s]
Pulse energy, E	5.0×10^{-4}	[J]
Absorption coefficient, η	0.2	–
Electron density, n_e	1.0×10^{20}	[cm^{-3}]
Numerical aperture, NA	0.45	–

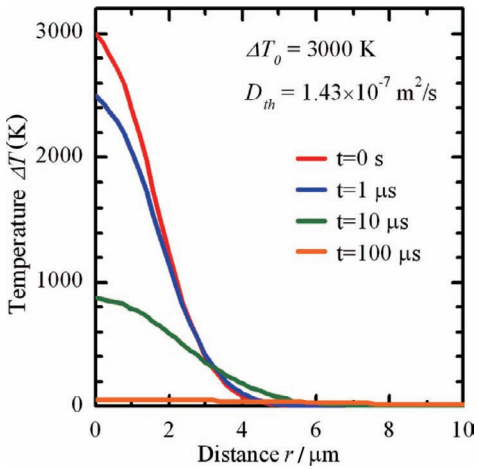

Fig. 6. Calculated temperature distributions just after the femtosecond single pulse irradiation as a function of the distance from focus. In this calculation, the time after the laser irradiation were changed from 0 s to 100 μs.

$$\Delta T(r,t) = \Delta T_0 \left(\frac{w_0}{\sqrt{w_0^2 + 4D_{th}t}} \right)^3 \exp\left(-\frac{r^2}{w_0^2 + 4D_{th}t} \right) \quad (8)$$

where ΔT_0 is the initial temperature just after the femtosecond single pulse irradiation, w_0 is the laser beam waist, t is the time after the irradiation, and r is the distance from the focus. **Figure 6** indicates the calculated temperature distributions just after the femtosecond single pulse irradiation as a function of the distance from focus. In this calculation, the time after the laser irradiation were changed from 0 s to 100 μs. Since the repetition rate of 1 kHz, i.e. the interpulse time of 1 ms in the experiments, these calculations apparently indicate that the heat induced by the first

pulse can diffuse away from the focal region before the arrival of the successive pulse. Indeed, no apparent temperature change occurred after the femtosecond laser irradiation for 60 min. The ZnO nucleation induced by the femtosecond laser irradiation could occur at the instantaneous high-temperature region surrounding the focal volume in precursor solution at room temperature.

4. Conclusions

In conclusion, ZnO nanorods have been successfully synthesized from heterogeneous nucleation initiated by femtosecond laser irradiation in aqueous solutions with subsequent hydrothermal treatments. Due to the localized high supersaturation of precursor solution, the size of the obtained hexagonal ZnO nanorods with femtosecond laser irradiation and the subsequent thermal treatment is about 4 times thinner than that obtained by the thermal treatment. Studies involving pH variation indicate that ZnO nucleus produced through different reaction pathways according to the pH value of the precursor solution. The size of the obtained hexagonal ZnO nanorods is variable according to the pH of the precursor solution. Apart from the fundamental importance of the mechanism of ZnO nucleation, the photo-initiated ZnO nucleation via femtosecond laser irradiation could be useful for chemical reaction in liquid phase.

Acknowledgments This work is partially supported by the New Energy and Industrial Technology Development Organization (NEDO), Grant-in-Aid for Scientific Research (20245043), and Nippon Sheet Glass Foundation for Materials Science and Engineering (NSG Foundation).

References

1) H. Ohta and H. Hosono, *Mater. Today*, 7, 42–51 (2004).
2) P.-F. Lin, C.-Y. Ko, W.-T. Lin and C. T. Lee, *Mater. Lett.*, 61, 1767–1770 (2007).
3) Y. C. Kong, D. P. Yu, B. Zhang, W. Fang and S. Q. Feng, *Appl. Phys. Lett.*, 78, 407–409 (2001).
4) M. H. Huang, S. Mao, H. Feick, H. Yan, Y. Wu, H. Kind, E. Weber, R. Russo and P. Yang, *Science*, 292, 1897–1899 (2001).
5) G. Sberveglieri, C. Baratto, E. Comini, G. Faglia, M. Ferroni, A. Ponzoni and A. Vomiero, *Sens. Actuators B*, 121, 208–213 (2007).
6) F. Zhang, X. Wang, S. Ai, Z. Sun, Q. Wan, Z. Zhu, Y. Xian, L. Jin and K. Yamamoto, *Anal. Chim. Acta*, 519, 155–160 (2004).
7) M. S. Arnold, P. Avouris, Z. W. Pan and Z. L. Wang, *J. Phys. Chem. B*, 107, 659–663 (2003).
8) E. Hosono, S. Fujihara, I. Honma and H. Zhou, *Adv. Mater.*, 17, 2091–2094 (2005).
9) C. J. Lee, T. J. Lee, S. C. Lyu, Y. Zhang, H. Ruh and H. J. Lee, *Appl. Phys. Lett.*, 81, 3648–3650 (2002).
10) Z. W. Pan, Z. R. Dai and Z. L. Wang, *Science*, 291, 1947–1949 (2001).
11) W. I. Park, D. H. Kim, S.-W. Jung and G.-C. Yi, *Appl. Phys. Lett.*, 80, 4232–4234 (2002).
12) Y. W. Heo, V. Varadarajan, M. Kaufman, K. Kim, D. P. Norton, F. Ren and P. H. Fleming, *Appl. Phys. Lett.*, 81, 3046–3048 (2002).
13) R. S. Wagner and W. C. Ellis, *Appl. Phys. Lett.*, 4, 89–91 (1964).
14) J. Zhang, L. Sun, C. Liao and C. Yan, *Chem. Commun.*, 3, 262–263 (2002).
15) X. Y. Zhang, J. Y. Dai, H. C. Ong, N. Wang, H. L. W. Chan and C. L. Choy, *Chem. Phys. Lett.*, 393, 17–21 (2004).
16) H. Q. Le, S. J. Chua, Y. W. Koh, K. P. Loh, Z. Chen, C. V. Thompson and E. A. Fitzgerald, *Appl. Phys. Lett.*, 87, 101908–1–3 (2005).
17) H. Zhang, D. Yang, X. Ma, Y. Ji, J. Xu and D. Que, *Nanotechnology*, 15, 622–626 (2004).
18) M. Yang, G. Pang, L. Jiang and S. Feng, *Nanotechnology*, 17, 206–212 (2006).
19) J. Zhang, L. D. Sun, J. L. Yin, H. L. Su, C. S. Liao and C. H. Yan, *Chem. Mater.*, 14, 4172–4177 (2002).
20) H. Adachi, K. Takano, Y. Hosokawa, T. Inoue, Y. Mori, H. Matsumura, M. Yoshimura, Y. Tsunaka, M. Morikawa, S. Kanaya, H. Masuhara, Y. Kai and T. Sasaki, *Jpn. J. Appl. Phys.*, 42, L798–L800 (2003).
21) H. Y. Yoshikawa, R. Murai, S. Maki, T. Kitatani, S. Sugiyama, G. Sazaki, H. Adachi, T. Inoue, H. Matsumura, K. Takano, S. Murakami, T. Sasaki and Y. Mori, *Appl. Phys. A*, 93, 911–915 (2008).
22) Y. Shimotsuma, T. Yuasa, H. Homma, M. Sakakura, A. Nakao, K. Miura, K. Hirao, M. Kawasaki, J. Qiu and P. G. Kazansky, *Chem. Mater.*, 19, 1206–1208 (2007).
23) E. T. Y. Lee, Y. Shimotsuma, M. Sakakura, M. Nishi, K. Miura and K. Hirao, *Mater. Lett.*, 62, 4044–4046 (2008).
24) E. T. Y. Lee, Y. Shimotsuma, M. Sakakura, M. Nishi, K. Miura and K. Hirao, *J. Nanosci. Nanotechnol.*, 9, 618–626 (2009).
25) S. Yamabi and H. Imai, *J. Mater. Chem.*, 12, 3773–3778 (2002).
26) S. Peulon and D. Lincot, *J. Electrochem. Soc.*, 145, 864–874 (1998).
27) A. Goux, T. Pauporté , J. Chivot and D. Lincot, *Electrochim. Acta*, 50, 2239–2248 (2005).
28) B. Hubert, N. Naghavi, B. Canava, A. Etcheberry and D. Lincot, *Thin Solid Films*, 515, 6032–6035 (2007).
29) Y. Zhang and J. Mu, *Nanotechnology*, 18, 075606–1–6 (2007).
30) S. Baruah and J. Dutta, *Sci. Technol. Adv. Mater.*, 10, 013001–1–18 (2009).
31) Z. Lin, L. V. Zhigilei and V. Celli, *Phys. Rev. B*, 77, 075133–1–17 (2008).
32) K. Hatanaka, T. Miura and H. Fukumura, *Chem. Phys.*, 299, 265–270 (2004).